Crustal structures of the northernmost South China Sea: Seismic reflection and gravity modeling

Yi-Ching Yeh and Shu-Kun Hsu
Institute of Geophysics, National Central University, Taiwan (E-mail: yeh@oc.gep.ncu.edu.tw)

Abstract

The South China Sea (SCS) is a marginal sea off shore Southeast Asia. Based on magnetic study, oceanic crust has been suggested in the northernmost SCS. However, the crustal structure of the northernmost SCS was poorly known. To elaborate the crustal structures in the northernmost SCS and off southwest Taiwan, we have analyzed 20 multi-channel seismic profiles of the region. We have also performed gravity modeling to understand the Moho depth variation. The volcanic basement deepens southeastwards while the Moho depth shoals southeastwards. Except for the continental margin, the northernmost SCS can be divided into three tectonic regions: the disturbed and undisturbed oceanic crust (8–12 km thick) in the southwest, a trapped oceanic crust (8 km thick) between the Luzon-Ryukyu Transform Plate Boundary (LRTPB) and Formosa Canyon, and the area to the north of the Formosa Canyon which has the thickest sediments. Instead of faulting, the sediments across the LRTPB have only displayed differential subsidence offset of about 0.5–1 s in the northeast side, indicating that the LRTPB is no longer active. The gravity modeling has shown a relatively thin crust beneath the LRTPB, demonstrating the sheared zone character along the LRTPB. However, probably because of post-spreading volcanism, only the transtension-shearing phenomenon of volcanic basement in the northwest and southeast ends of the LRTPB can be observed. These two basement-fractured sites coincide with low gravity anomalies. Intensive erosion has prevailed over the whole channel of the Formosa Canyon.

Introduction

The northernmost South China Sea (SCS) is bounded by the Eurasian continental margin, the Taiwan orogenic belt and the Manila subduction system (Figure 1). There are several models proposing the evolution and formation of the oceanic crust of the SCS. For instance, Taylor and Hayes (1980, 1983) proposed that the SCS was formed during 32–17 Ma (magnetic anomaly C11–C5d). Based on the magnetic data compiled by Chen (1987), Briais et al. (1993) further elaborated that the ages of the SCS oceanic crust could be 32–15.5 Ma (magnetic anomaly C11–C5c). Nevertheless, due to lack of data, the northernmost area of the SCS was rarely studied. Recent marine magnetic data shows that the northernmost SCS contains several almost E–W trending magnetic lineations, belonging to oceanic crust and the age could be as old as 37 Ma (Magnetic anomaly C17) (Hsu et al., 2005) (Figure 1). Therefore, the existence of the oceanic

crust of the SCS is extended northwards to north latitude N21°30′ in the offshore area of the southwest Taiwan.

Morphologically, the northernmost SCS is marked by the presence of the Formosa Canyon and some distributed seamounts (Figures 1 and 2) (Liu et al., 1998; Hsu et al., 2005). The northwestern, upstream portion of the Formosa Canyon has developed along a topographic escarpment with a vertical offset of about 300 m (Hsu et al., 2005). It is suggested as the northwestern portion of an extinct transform fault named the Luzon–Ryukyu Transform Plate Boundary (LRTPB) (Sibuet et al., 2002; Hsu et al., 2005). The LRTPB is supposed to be the southwestern termination of the former Ryukyu Trench (Hsu and Sibuet, 1995; Sibuet and Hsu, 1997, 2005). However, the crustal structures of the LRTPB and the northernmost SCS are still poorly known. In this paper, we use seismic reflection and gravity anomaly data to elaborate the crustal structures of the northernmost SCS and off southwest Taiwan.
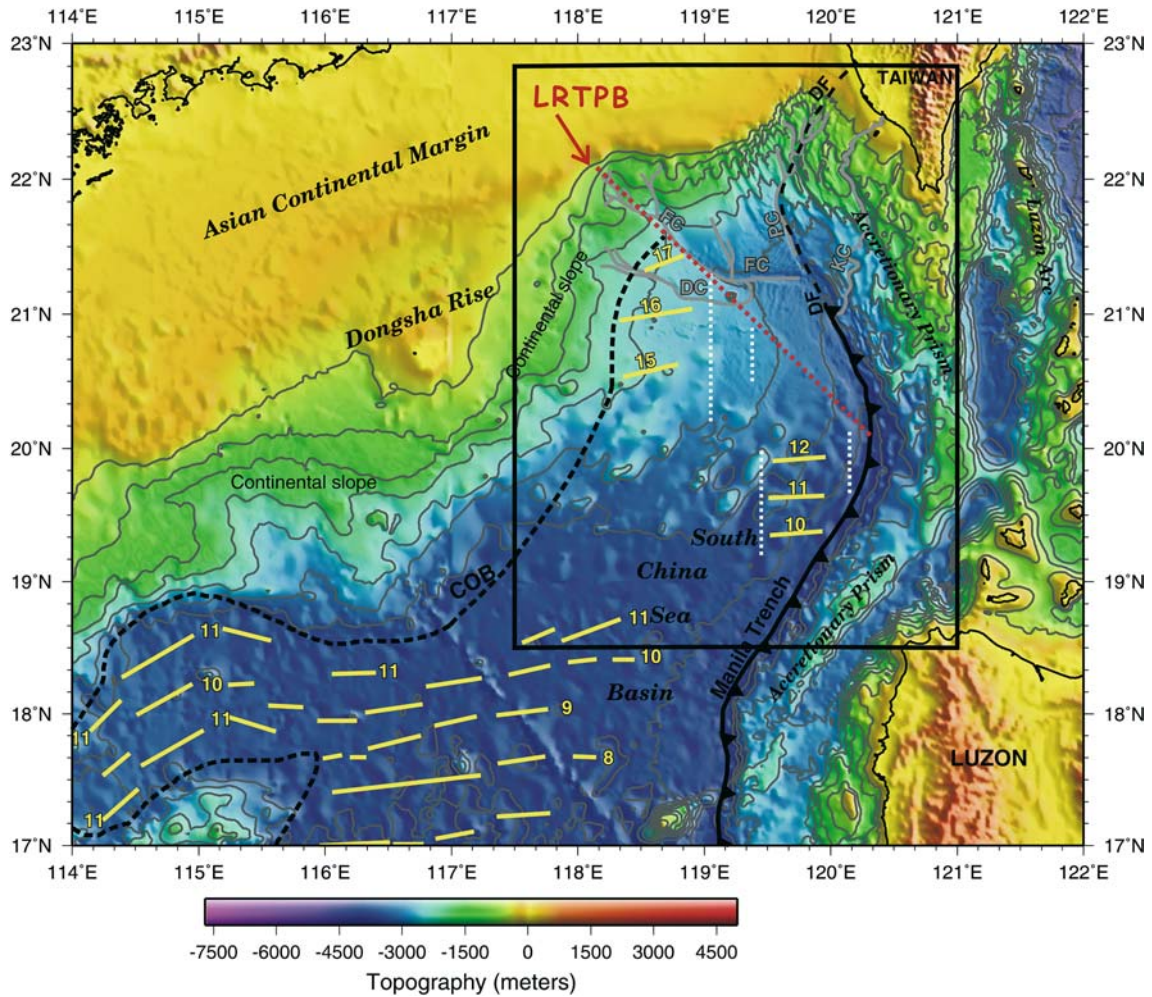
Figure 1. Tectonic setting of the northern SCS, superimposed on the bathymetry. The yellow lines are magnetic lineations identified by Briais et al. (1993) (south of 19°N) and Hsu et al. (2005) (north of 19° N). Inset is the study area. The red dashed line indicates the suggested boundary of the northern SCS oceanic crust (LRTPB) and the white dashed lines are the old fractured zones of the SCS suggested by the magnetic anomaly (Hsu et al., 2005). The gray lines indicate submarine canyons. KC: Kaoping Canyon; PC: Penghu Canyon; FC: Formosa Canyon; DC: Dongsha Canyon; DF: deformation front.

Data and processing

In 1996, the ACT cruise collected eight seismic reflection profiles of six channels across the middle portion of the LRTPB (Lallemand et al., 1997; Sibuet et al., 2002) (Figure 2). A streamer of 240 m and a GI Gun source of 150 c.i. volume with 10 knots ship speed were used. To have a comprehensive understanding of the structure and characteristics related to the LRTPB sheared zone, we used the R/V Ocean Research I to conduct two supplementary seismic reflection surveys (the ORI645 and ORI689 cruises) across the northern and southern portions of the LRTPB zone. The ORI645 cruise provides 24-channel seismic profiles that are generally perpendicular to the upstream of the Formosa Canyon, while the ORI689 cruise provides 48-channel seismic profiles (Figure 2). Besides, two seismic profiles (ORI689-5 and mltw) across the Eurasian continental margin and SCS basin (Tsai et al., 2005) are also included for interpretation (Figure 2). The seismic acquisition parameters in ORI645 and ORI689 cruises are the same and they contain a group interval of 12.5 m, total air gun source volume of the 1275 c.i. (500 c.i. +
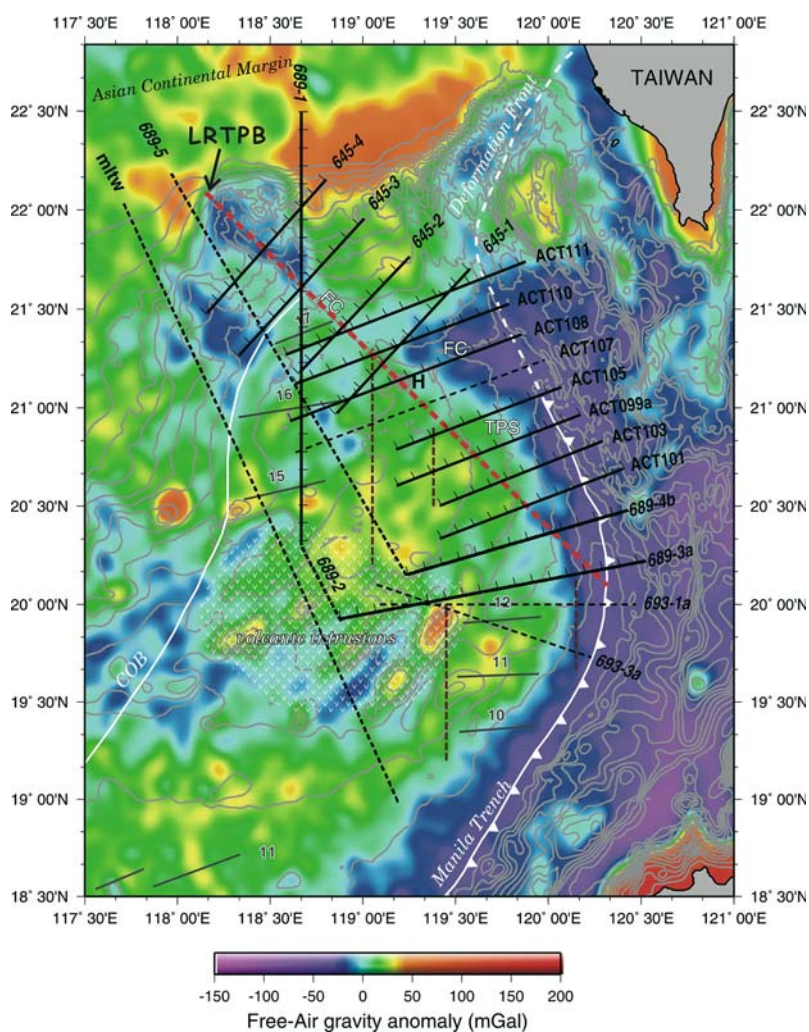
Figure 2. Locations of the 20 seismic reflection profiles used in this study. Bathymetric contours of 200 m interval are plotted. The free-air gravity anomaly is draped on the bathymetry. The volcanic intrusion zone is marked by v-shaped pattern. The red dashed line indicates the LRTPB location; the brown dashed lines are the SCS fractured zones (Hsu et al., 2005); the gray lines are magnetic lineations as shown in Figure 1. FC: Formosa Canyon; TPS: a trapped oceanic crust of the Philippine Sea plate (Hsu et al., 2005).

500 c.i. + 275 c.i.), a ship speed of 5 knots, a shot interval of 20 s (about 50 m), a sampling rate of 2 ms and a record length of 10 s. In total, 20 seismic reflection profiles are used in this study. We have used both ProMAX and SIO-SEIS seismic software to process the seismic reflection data with Ultra Sun Sparc IIi and Linux Workstations. Due to the short offset (240 m) and high ship speed (10 Knots), the eight ACT profiles have only been applied a 8–16–32–64 Hz band-pass filter tapering at both ends, a 500 ms moving window AGC, and a water velocity (1480 m/s) stacking. The four ORI645 profiles

have been processed with 8–16–60–120 Hz band-pass filter, 60 Hz notch filter, minimum phase predictive deconvolution and water velocity (1480 m/s) stacking. The four ORI689 (MCS689-1 to MCS689-4) and the two ORI693 (MCS693-1a and MCS693-3a) profiles have been processed with the similar parameters as the ORI645 profiles but have been applied water velocity 1480 m/s time migration. Only the seismic profiles indicated by solid lines in Figure 2 are shown in this paper (Figures 3–16).

To understand the Moho depth variation and crustal thicknesses in this area, we have calcu-
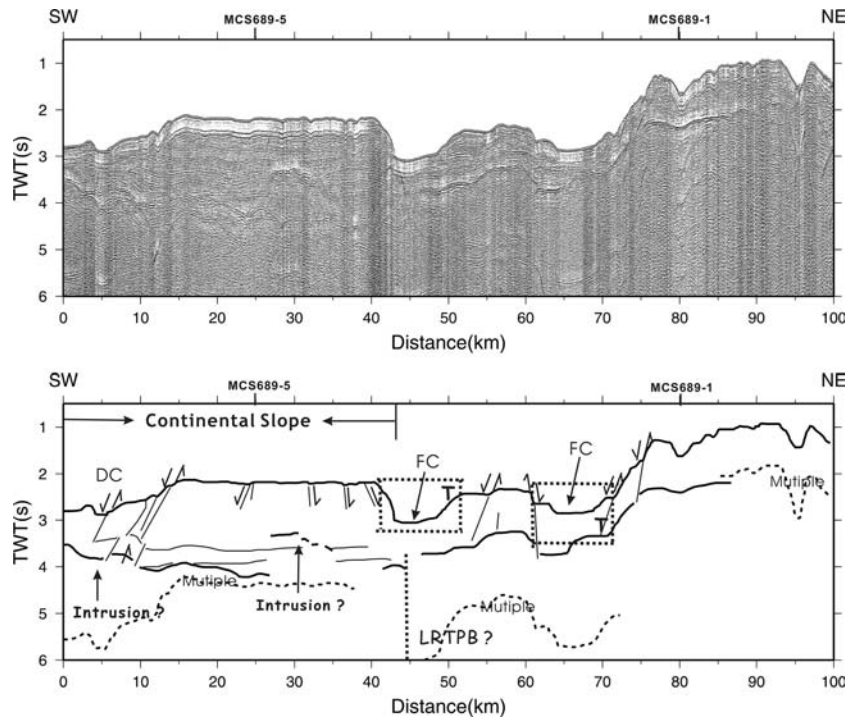
Figure 3. MCS645-4 stacked seismic profile and its interpretation. The sediment layers have been obviously truncated at the Formosa Canyon (box T in Figure 3 and in the following figures). FC: Formosa Canyon.
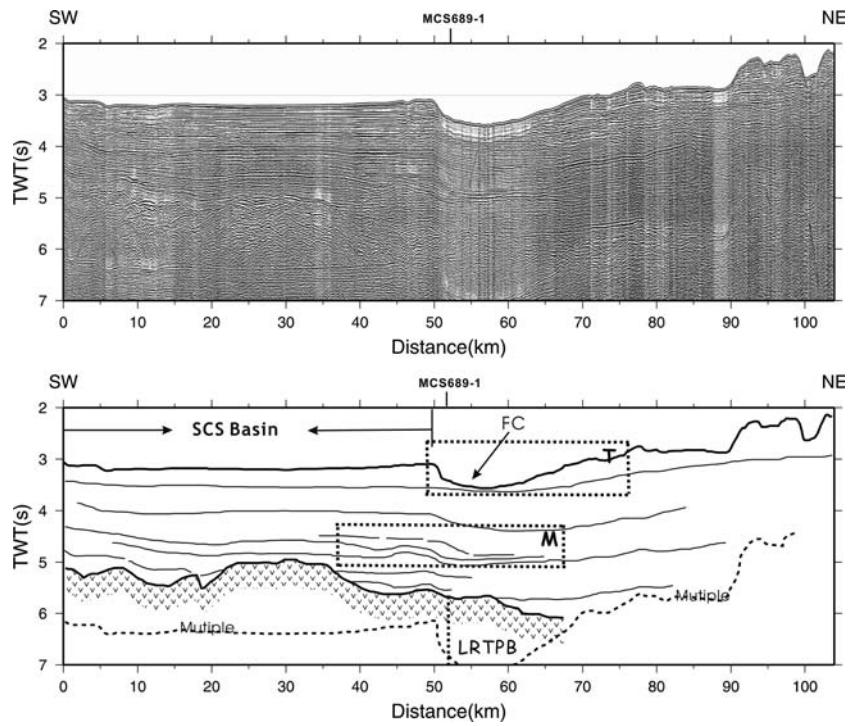
Figure 4. MCS645-3 stacked seismic profile and its interpretation. Possible debris flow zone in box M is suggested above the LRTPB.
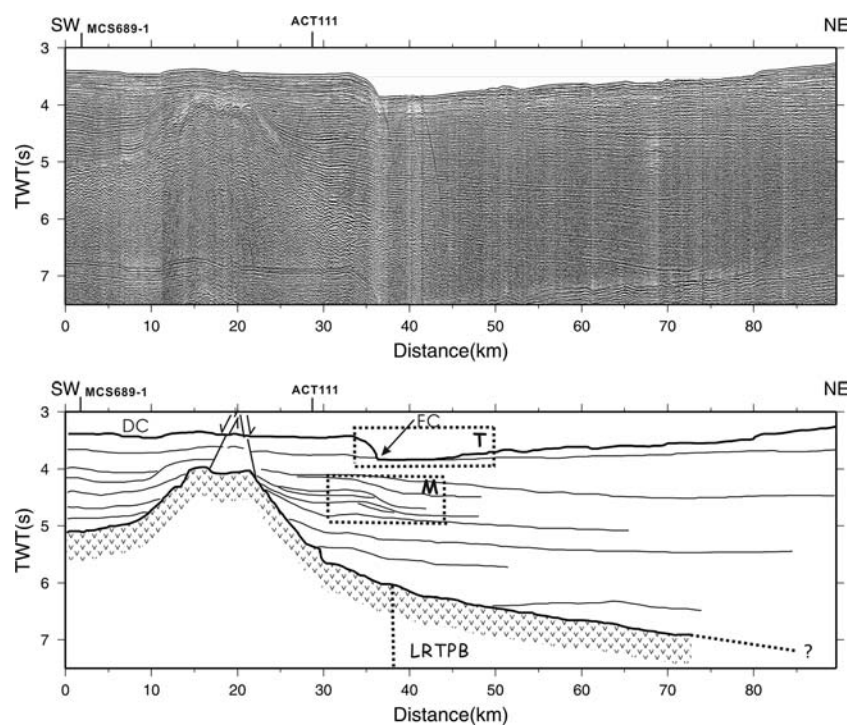
Figure 5. MCS645-2 stacked seismic profile and its interpretation.
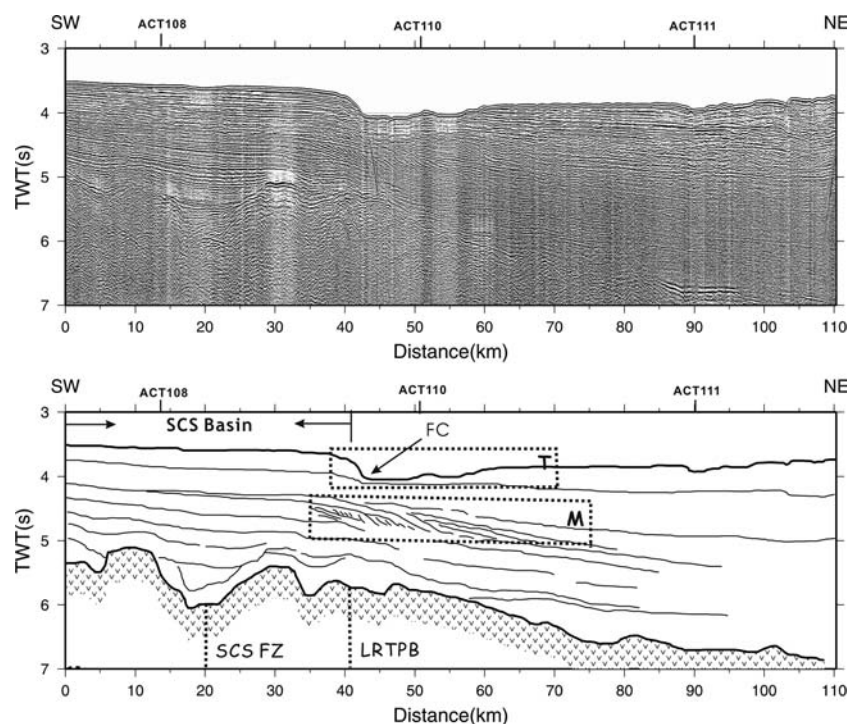
Figure 6. MCS645-1 stacked seismic profiles and its interpretations. Noted that the basement depth deepens gradually toward the north and the overlying sediment layers have been bent also downwards in the north.
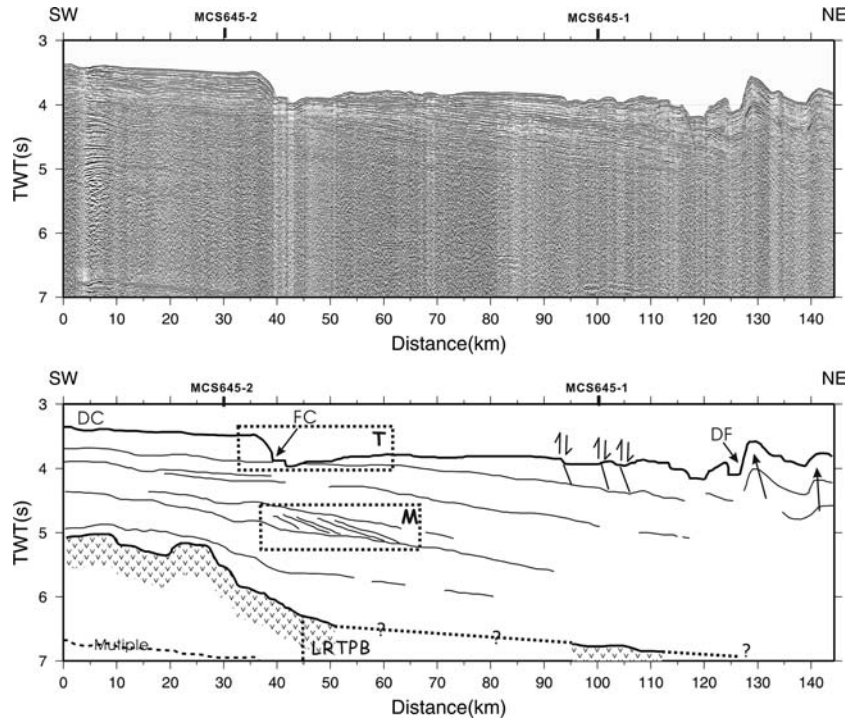
Figure 7. ACT111 stacked seismic profile and its interpretation.
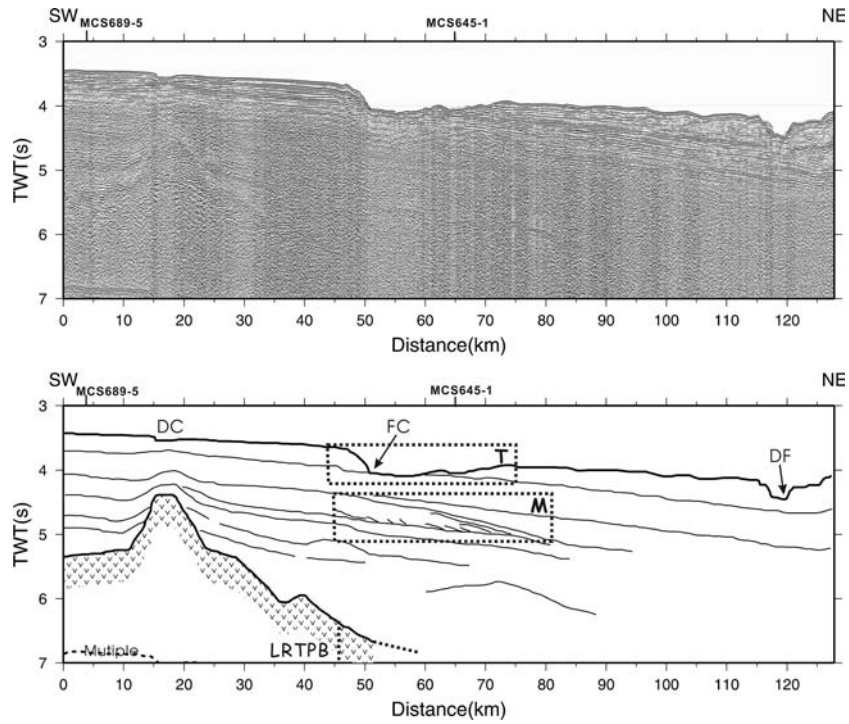
Figure 8. ACT110 stacked seismic profile and its interpretation.
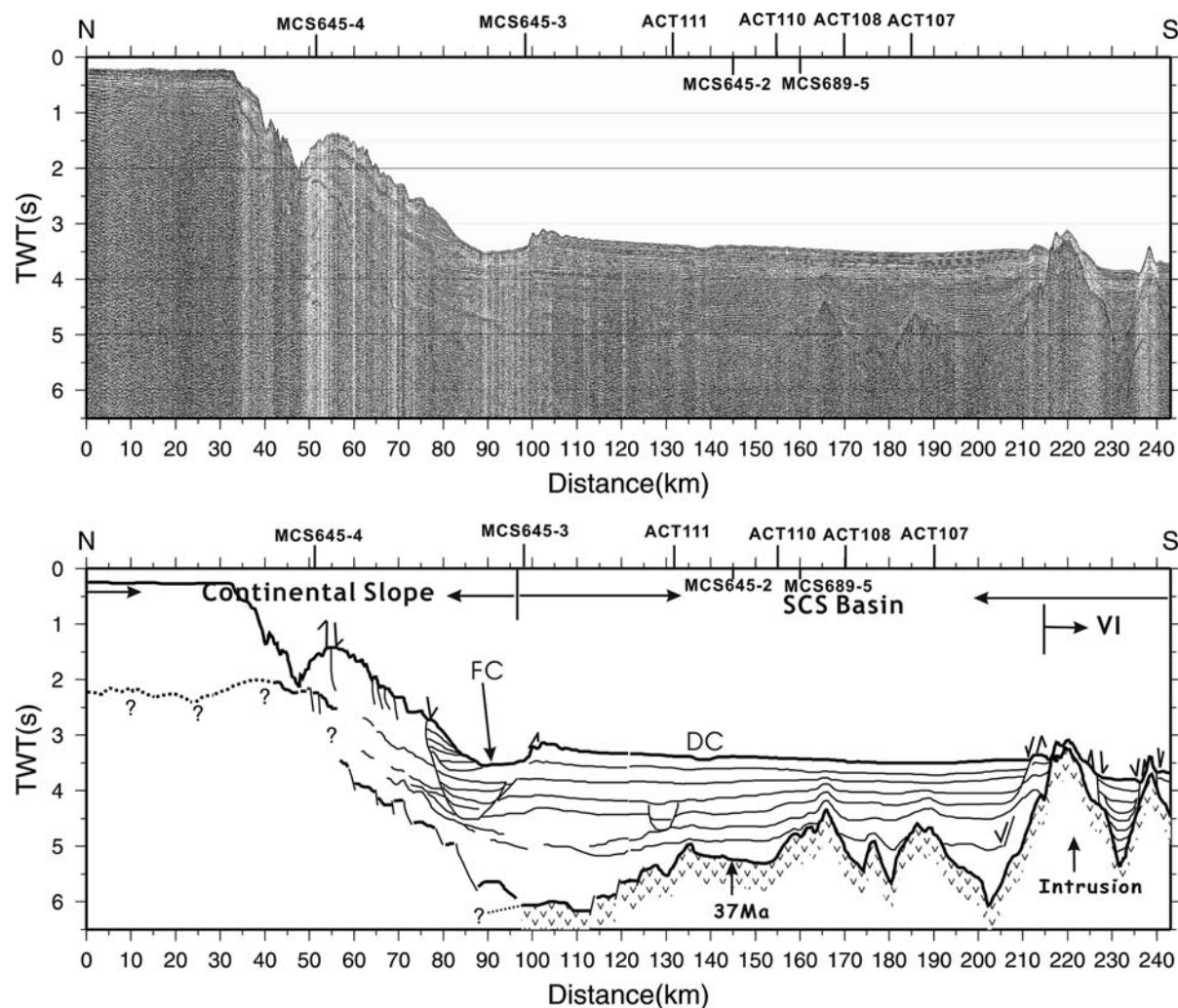
Figure 9. MCS689-1 migrated seismic profiles and its interpretation. Noted that the basement displays an obvious normal faulting at the distance near 100–130 km. The faulting location also marks the transition zone between the continental margin and the oceanic crust.

lated the Bouguer gravity anomaly. To estimate the gravity effect caused by the water and sediment layers, we have used the water density $\rho_w = 1.03$ g/cm^3, sediment density $\rho_s = 2.2$ g/cm^3 and the crust density $\rho_c = 2.85$ g/cm^3. Each block of 2 km $\times$ 2 km is used to calculate the gravity effect from the upper crustal structures. After reducing the gravity effect of the two interfaces (seafloor and volcanic basement) from the free-air gravity anomaly (Hsu et al., 1998), the Moho discontinuity Bouguer gravity anomaly map is obtained (Figure 17). In fact, the calculated Bouguer anomaly reflects the relief of the Moho depths that generally shoal southeastwards.

Structural interpretation along seismic profiles

The Formosa Canyon changes its orientation from NW–SE to W–E near a submarine volcano (symbol H in Figure 2). The NW-SE trending segment of the Formosa Canyon has developed along the LRTPB and show an obvious escarpment (Hsu et al., 2005). Most of the seismic profiles used in this study have crossed the LRTPB. For simplicity, we divide the seismic profiles into two groups: group A and group B. The group A contains the profiles in the northwest side of the seamount H, while the group B contains profiles in the southeast side. The seismic profiles of
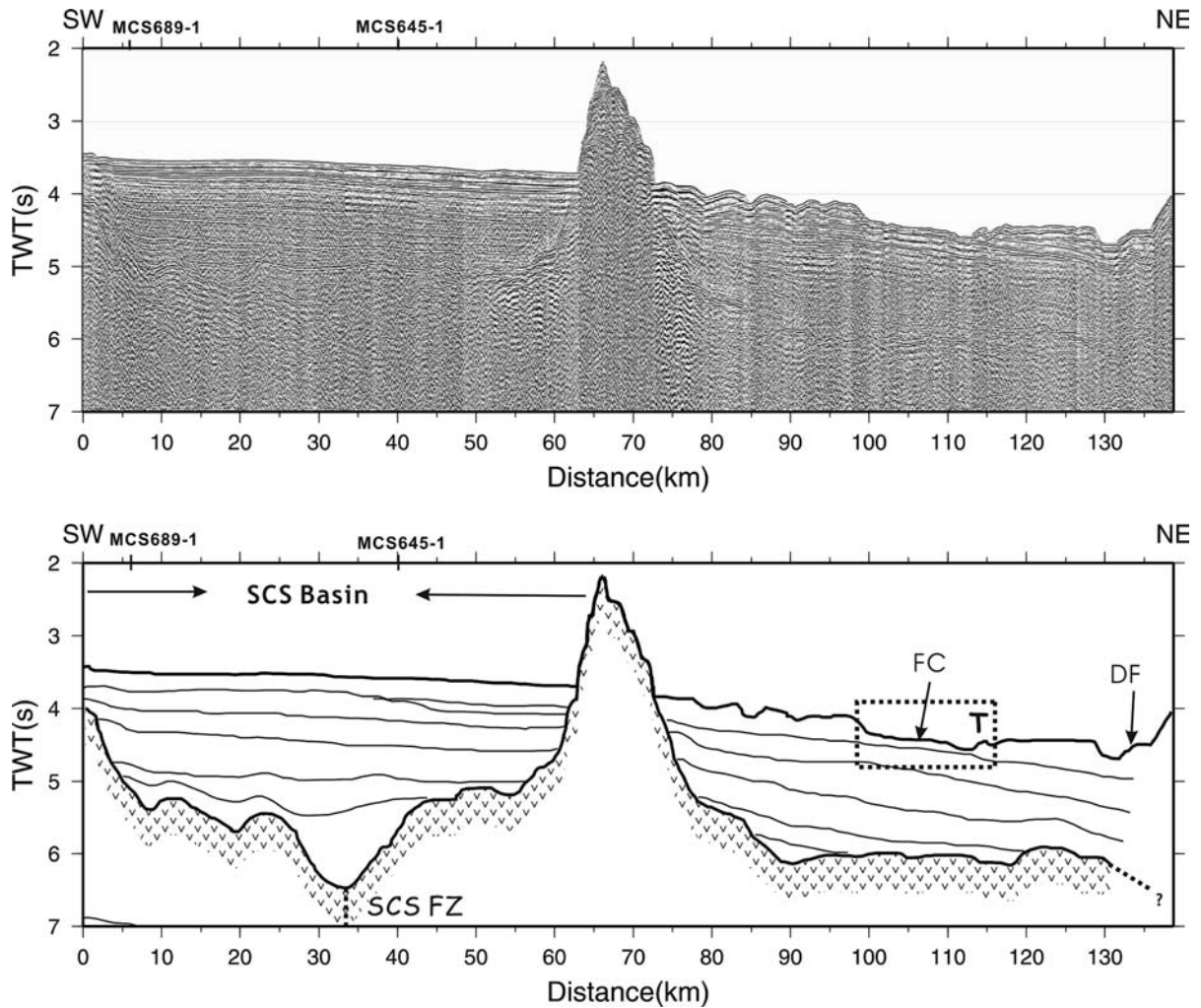
Figure 10. ACT108 stacked seismic profile and its interpretation. This profile is directly over the seamount H (Figure 2). DF: deformation front

group A generally cross the continental margin and/or the SCS oceanic basin. The seismic profiles of group B generally cross the SCS oceanic basin, a trapped piece of oceanic crust (Hsu et al., 2005) and the Manila Trench.

Seismic profiles across the northwest portion of the LRTPB (group A)

MCS645-4 stacked profile (Figure 3)
The profile MCS645-4 is located on the continental slope (Figure 2). Several normal faults have occurred in the upper sediments (less than 3.5 s TWT). Truncation of the seismic sequences, indicating an erosion environment along the channel,

clearly exists across the Formosa Canyon (box T in Figure 3). Probably due to the thick sediment, the volcanic basement is not recognized. A high amplitude seismic sequence, however, is observed between 3 and 4 s TWT. Non-continuous reflection phase and re-activated thrust faults in deep layers may indicate volcanic intrusions below the Dongsha Canyon area (Figure 3).

MCS645-3 stacked profile (Figure 4)
The profile MCS645-3 lies almost along the base of the continental slope (Figure 2). The channel of the Formosa Canyon has been extensively eroded as evidenced by the truncation of the upper seismic sequences. As a matter of fact, this
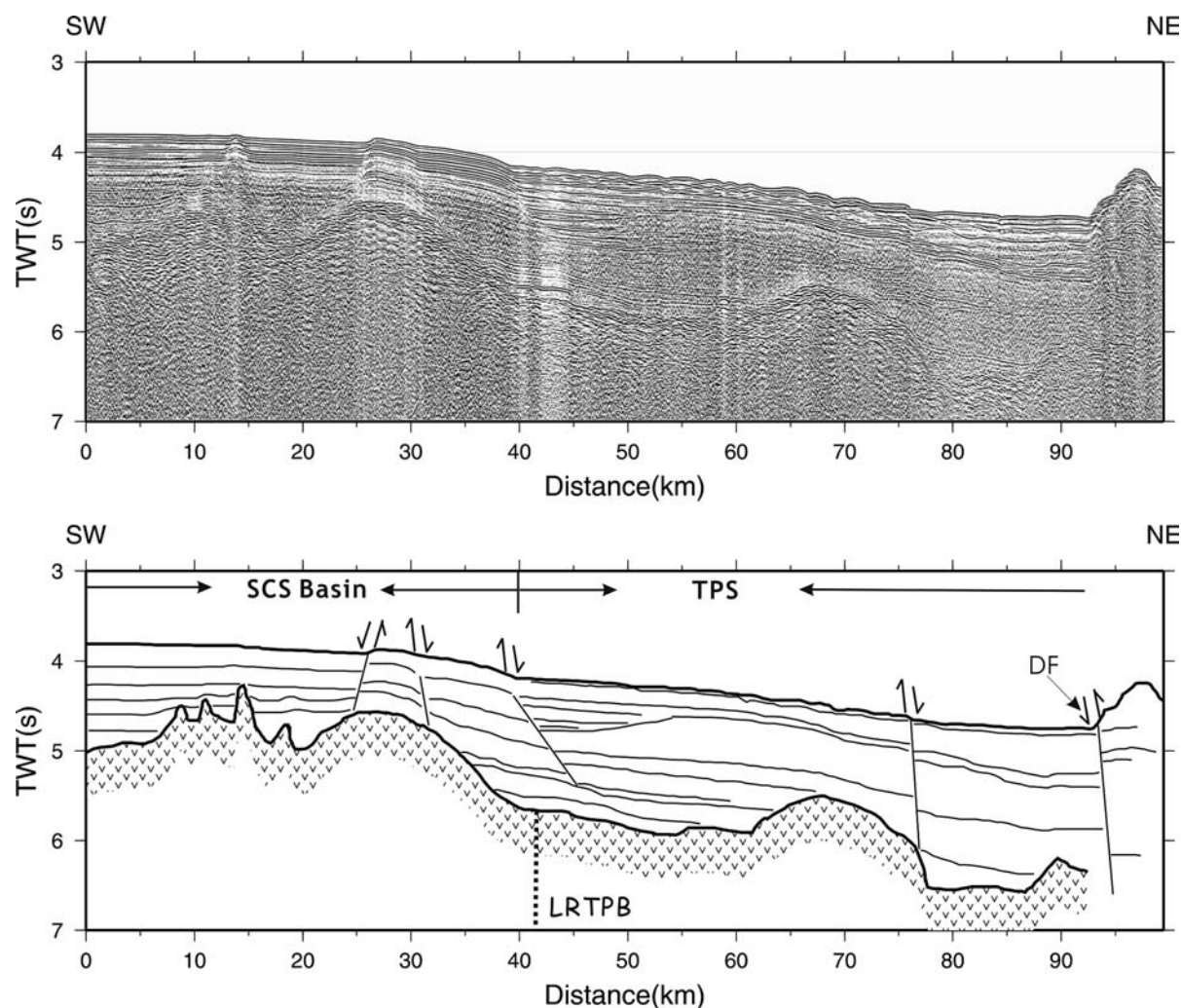
Figure 11. ACT105 stacked seismic profile and its interpretation. Noted that the basement depth levels are slightly different on either side of the LRTPB. Close to the deformation front, the overlying sediments have been cut by normal faulting from the top surface to the basement. TPS: a trapped piece of oceanic crust.

erosion phenomenon is true along the whole channel of the Formosa Canyon (Figure 18). The volcanic basement (probably of continental origin or volcanic intrusion) is observed in the southern side at depth of about 5 s TWT and deepens gradually toward the north. Beneath the Formosa Canyon, the seismic sequences at 4–5 s TWT obviously bent downwards toward the north. It could be caused by differential subsidence on both sides of the LRTPB or a duplex (in block M of Figure 4). Because this feature is observable beneath the Formosa Canyon and can be found in all the profiles in the north of the seamount H (in block M of Figures 4–6), it

seems to be a northward slumping or debris flow zone. Considering the volcanic basement of 37 Ma in this area (see profile MCS689-1 in Figure 16) (Hsu et al., 2004), the sedimentation rate is, on average, ca. 52 m/My. Hence, the occurrence age of the possible debris flow is close to the 22 Ma of the seamount H dated by Ar–Ar method (Hsu et al., 2005). We conclude that the northwestward debris flow was due to the volcanic extrusion of the seamount H (Figure 18).

MCS645-2 stacked profile (Figure 5)
Profile MCS645-2 lies to the south of MCS645-3 and nearly parallel to the MCS645-3 (Figure 2).

54
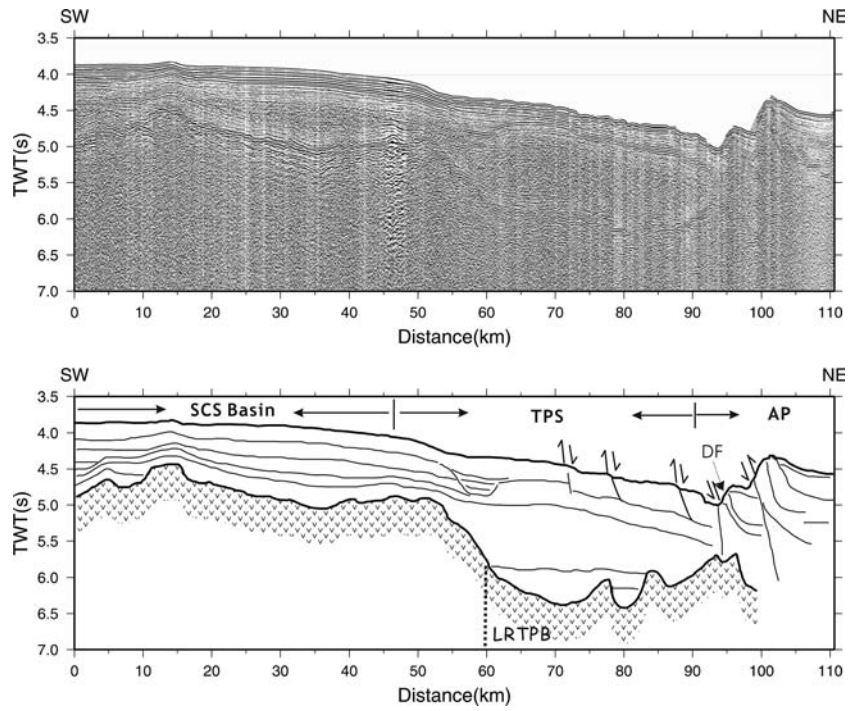
Figure 12. ACT099a stacked seismic profile and its interpretation. This profile has similar basement drop as in Figure 11. AP: accretionary prism
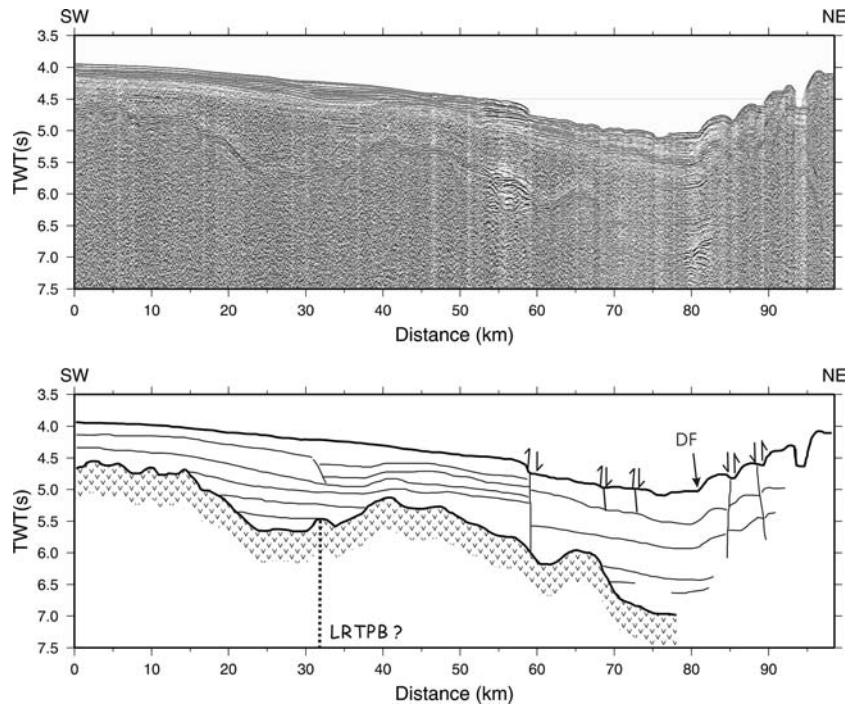
Figure 13. ACT103 stacked seismic profile and its interpretation.
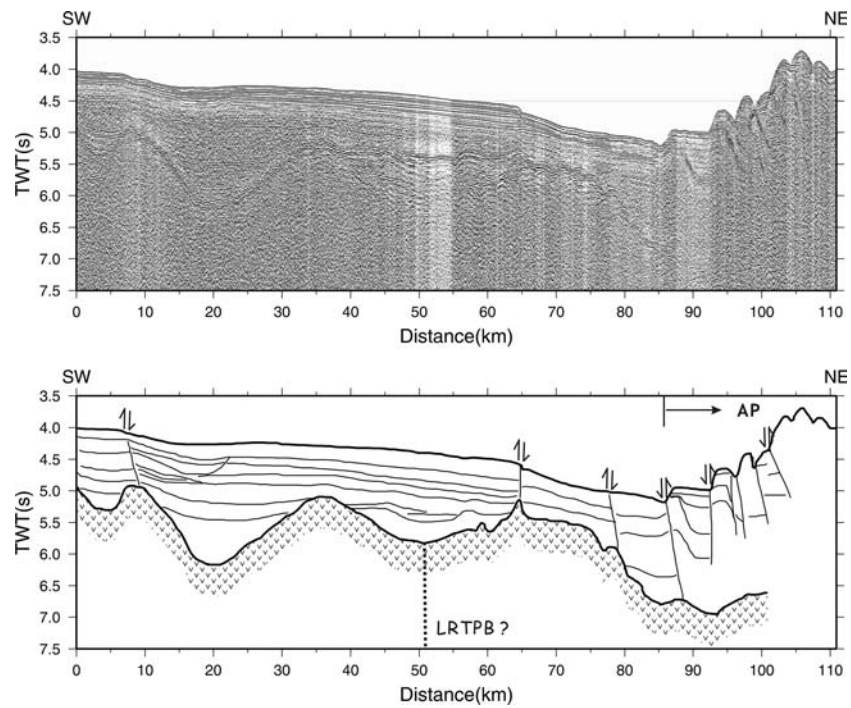
Figure 14. ACT101 stacked seismic profile and its interpretations.
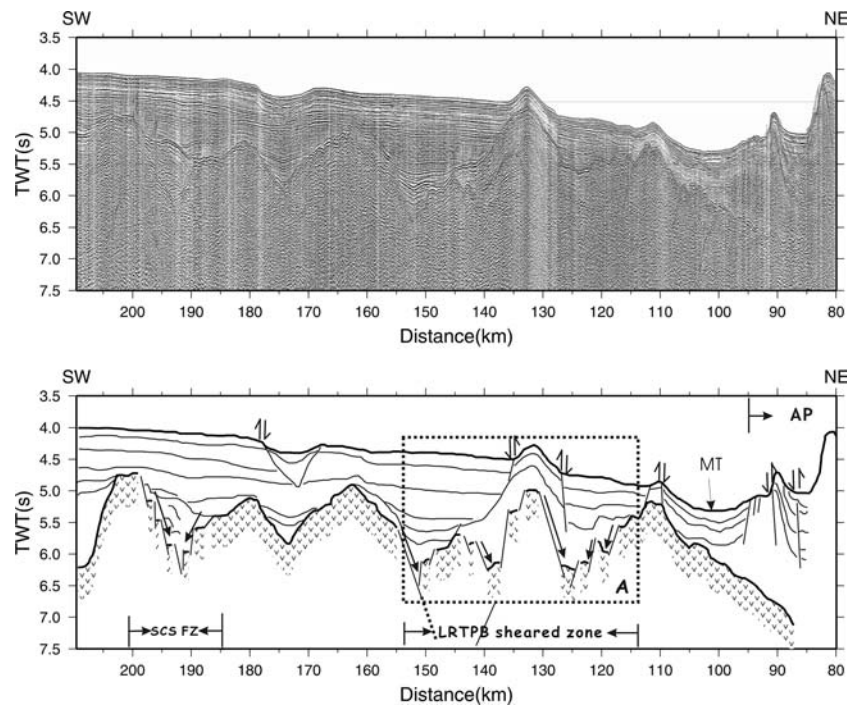
Figure 15. MCS689-4b migrated seismic profile and its interpretation. Box A indicates the location of the sheared zone of the LRTPB. FZ: fracture zone. MT: Manila Trench.
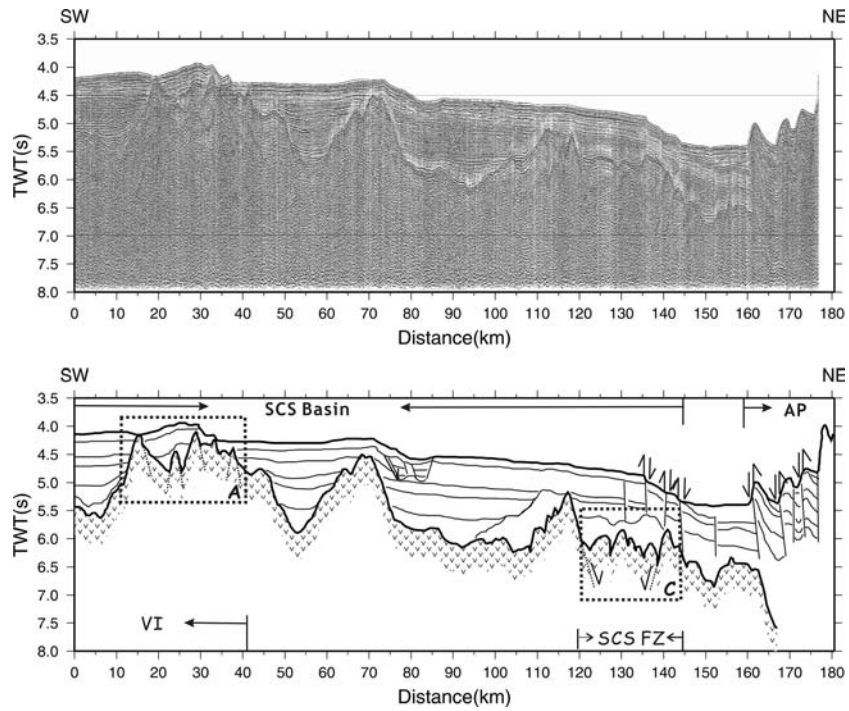
Figure 16. MCS689-3a migrated seismic profile and its interpretation. VI: volcanic intrusion zone.

The truncation of seismic sequences at the Formosa Canyon and the debris flow beneath the Formosa Canyon can be clearly observed (Figure 5). A volcanic, intrusive basement high is observed at distance 15 km of profile MCS645-2, and the basement also goes down gently toward
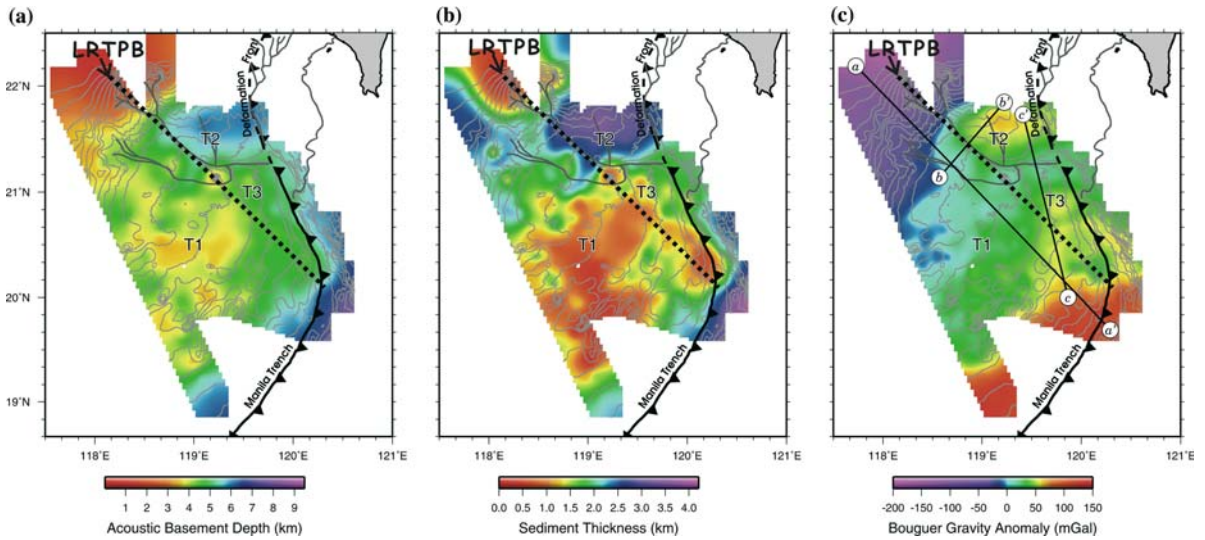
Figure 17. (a) The basement depth map. Note that the basement depths for the regions T2 and T1 are strikingly different. (b) The sediment thickness map. The thickest sediment zone occurs in the region T2. (c) The Moho discontinuity Bouguer anomaly map. The region T2 shows a relatively high anomaly (∼50–60 mGal) than in the south side of the LRTPB and is separated from the region T3 by the Formosa Canyon.
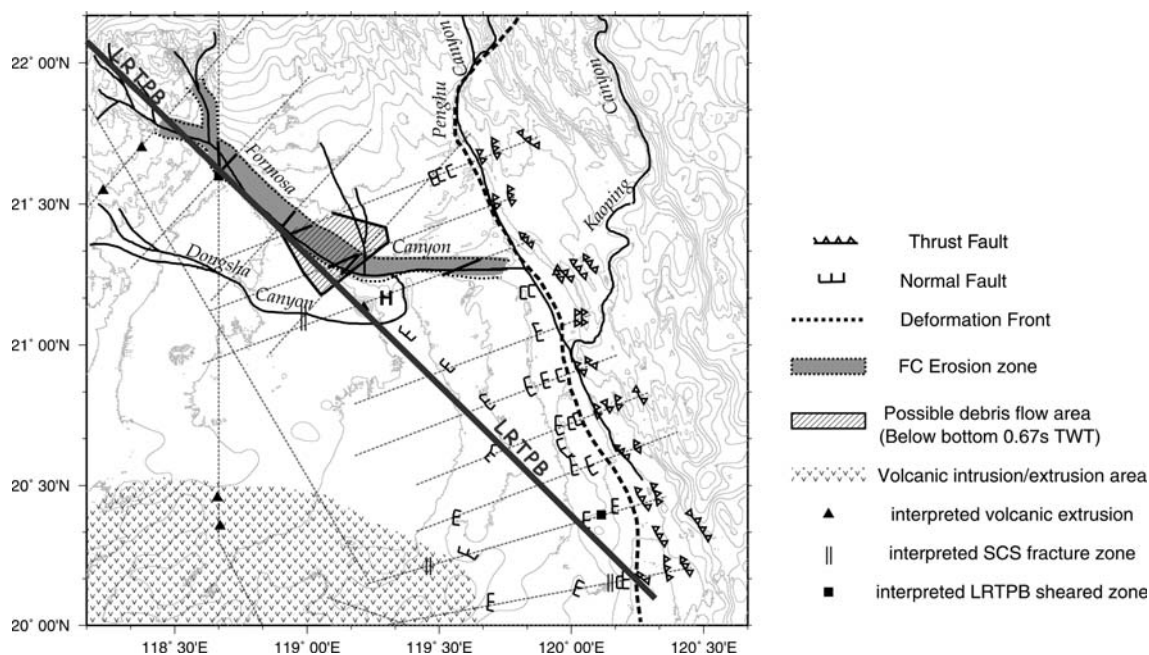
Figure 18. Structures interpreted by the used seismic profiles, superposed on the bathymetric contours map. Noted that the erosion occurs along the whole channel of the Formosa Canyon. The possible debris flow zone is possibly associated with volcanic intrusion of the seamount H. The deformation front is defined by the distinction between the normal faults and the thrust faults.

the north (Figure 5). To the south the volcanic basement should be of oceanic crust; however, the characters of oceanic crust are only suggested in profile MCS689-1 (Figure 9).

MCS645-1 stacked profile (Figure 6)
Profile MCS645-1 is also NE–SW trending and is located from the SCS basin to the base of the continental slope (Figure 2). The basement depth deepens toward the north. The truncation of seismic sequences at the Formosa Canyon is still observable. A basement depression is observed near distance 20 km where the free-air gravity anomaly is low (Figure 2). This location may correspond to a SCS fracture zone as evidenced by the magnetic anomaly (Figure 2) (Figure 4 of Hsu et al., 2005). The magnitude of the possible volcanic debris flow layer beneath the Formosa Canyon (in box M of Figure 6) is the largest in all the profiles available.

ACT111 and ACT110 stacked profiles (Figures 7 and 8)
Profiles ACT111 and the ACT110 have similar seismic structures as the previous profiles. The basement deepens northwards and the sediment

thickness becomes larger in the northern side of the LRTPB. The truncation of the top layers of the sediments beneath the Formosa Canyon and the possible debris flow zone beneath the LRTPB zone still exist. Some normal faults near the deformation front are observed.

MCS689-1 migrated profile (Figure 9)
This N–S trending profile starts from the Asian continental margin, through the LRTPB, then into the SCS basin (Figure 2). The Continent–Ocean boundary is probably located at the distance 100 km at a depth of 6 s TWT. The overlying sediments indicate that the LRTPB is an old feature. The basement was obviously fractured into several blocks and deepens towards the continental margin. At distance 200–245 km, volcanic intrusions probably exist, as observed by the normal faults on the flanks of the intrusions (area VI in Figure 9).

Seismic profiles across the southeast portion of the LRTPB (group B)

ACT108 stacked profile (Figure 10)
This profile ACT108 crosses a possible SCS fracture zone and the seamount H and ends at the

deformation front or the Manila accretionary prism (Figure 2). The negative Bouguer anomaly over seamount H indicates an existing root of the volcano (Figure 17c). Probably because of this later volcanism the basement shearing related to the LRTPB is not observed. The truncated sediment layer through the downstream of the Formosa Canyon can still be observed. A possible location of SCS fracture zone displays a basement depression at the distance ca. 33 km (Figure 10).

ACT105, ACT099a, ACT103 and ACT101 stacked profiles (Figures 11–14)

The post-spreading volcanism along parts of the LRTPB area (Sibuet et al., 2002) has probably smoothed the basement offset across the LRTPB. However, profiles ACT105 and ACT099a have shown a slight difference in the basement depths on either side of the LRTPB (Figures 11 and 12). Because the northern ends of the profiles are located above the deformation front, normal faulting due to the lithospheric bending of the SCS lithosphere can be discerned (Figures 11–14). To the northeast of the deformation front, the stress has changed from extension to compression; the thrust faulting becomes prominent in the accretionary prism.

MCS689-4b migrated profile (Figure 15)

This profile goes through a SCS fracture zone and stops at the Manila subduction complex (Figure 2). At the distance between 115 and 155 km, the basement was sheared into several blocks (Figure 15). However, young seismic sequences seem not to be associated with the basement faulting. Another crustal fractured area appears at distance 185–205 km. The crust was also faulted into several blocks, but normal faults did not affect the oldest sediment layer. Therefore, we interpret it as one of the SCS oceanic fracture zones (Figure 15).

MCS689-3a migrated profile (Figure 16)

On this profile, volcanic intrusions are found in box A. These intrusions probably occurred after spreading of the SCS oceanic crust. In box C, basement faulting is observed. Because this faulting zone appears in the line of a SCS fracture zone identified by magnetic anomaly (Hsu et al., 2005) (Figure 2), it probably belongs to a SCS fracture zone. The LRTPB sheared zone is supposed to appear to the right of this fracture zone. The supposed LRTPB is probably located beneath the Manila Trench (cf. Figures 2 and 16); therefore, the LRTPB is not recognized in profile MCS689-3a. The bending of the subducted lithosphere and the transition (deformation front) from extension to compression can be observed at the distance of about 155 km. (Figure 16).

Tectonic features of the LRTPB sheared zone

Although the seafloor shows a large escarpment along the northwestern portion of the LRTPB, the corresponding volcanic basement does not show a sharp discontinuity across the LRTPB. However, the basement displays gentle dipping towards southwest Taiwan (Figure 17a). Thick sediments exist to the right of the LRTPB and are limited in the south by the Formosa Canyon (region T2 in Figure 17b).

In contrast, in the southeast of seamount H, the bathymetry shows a slight offset, normal faulting dipping to the northeast, along the southeast portion of the LRTPB (Figure 18). In this portion, the offset of ca. 1 s TWT of the basement level on both sides of the LRTPB can be observed (Figures 10 and 11). However, no clear faults have cut across the entire sediments above the LRTPB, which indicate that the transform fault was extinct before the deposition of the overlying sediments. Some deformation is probably due to the different cooling effects of the basement on either side of the LRTPB. Normal faults cutting through the whole sediments do occur near the Manila Trench; however, they are probably due to the bending of the subducted lithosphere (Figures 11, 13 and 14).

It is worth noting that the shearing characteristics along the LRTPB can only be observed at both ends of the transform fault (Figures 9 and 15). Both shearing places are marked by relatively low gravity anomalies (Figure 2). The shearing at the northwest end of the LRTPB has occurred at the crustal contact between the SCS oceanic crust and the Asian continental crust (Figure 9). On the other hand, the shearing along the southeast end of the LRTPB was between oceanic crusts (Figure 15). The base-
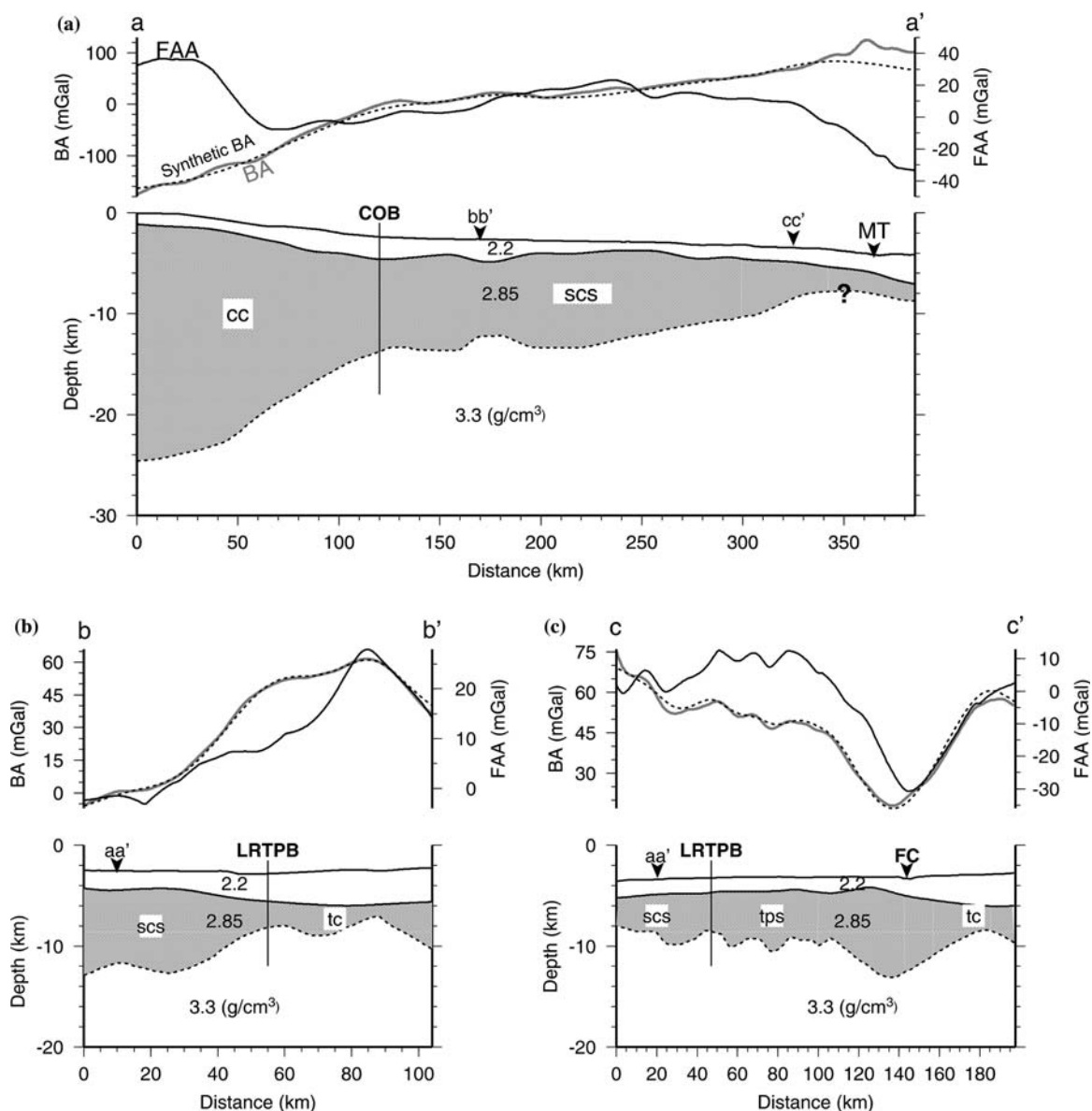
Figure 19. The Moho depth variation calculated by the forward gravity modeling. The locations of the three profiles (aa', bb' and cc') are shown in Figure 17c. The black bold line is the free-air gravity anomaly. The gray dashed line is the Bouguer anomaly (BA) extracted from the 3D Bouguer anomaly in Figure 17c. The dashed line is the synthetic Bouguer anomaly. cc: continental crust; scs: South China Sea; tc: thinned continental crust; tps: trapped Philippine Sea oceanic crust; LRTPB: Luzon Ryuku Transform Plate Boundary; FC: Formosa Canyon; MT: Manila Trench.

ment along the LRTPB was sheared and deformed into several normal faulting blocks (from distance 115 to 155 km in Figure 15). The existence of the inactive normal faults in the basement suggests that the plate boundary along the LRTPB was probably under a transtension mechanism.

Crustal characteristics of the Northernmost SCS

To understand the sediment thickness and the basement depth distribution, we have converted the seismic time (TWT) sections into depth (kilo-meters) sections by using a water velocity of 1500 m/s and an average sediment velocity of

2200 m/s. Based on the results and the location of the LRTPB, we can divide the northernmost SCS into three regions (T1, T2 and T3 in Figure 17) separated by the LRTPB and the Formosa Canyon. The depth to the basement of the SCS basin (T1) is about 3.5–4.5 km. The basement generally shoals toward the continental side and deepens toward the Manila Trench (Figure 17a). However, the average basement depth difference between T1 and T2 is obvious (Figure 17a); in the T2 region, the basement is about 5–7 km deep while it is 4.5–5.5 km deep in the T1 region. The overlying sediments are very thick in the T2 region (Figure 17b), which may be related to the loading in the Taiwan orogen and flexure of the continental margin (Lin and Watts, 2002). For the T1 region, the sediments are thicker both on the continental margin and trench sides but thinner in the middle of T1 region (1.0–1.75 km) (Figure 17b).

The Moho discontinuity Bouguer anomaly in the northernmost SCS generally displays low values in the northwest continental side and high values in the southeast trench side (Figure 17c). It indicates that the upper mantle or the Moho surface shoals towards the Manila Trench. In other words, the crust generally becomes thinner southeastwards as evidenced by the gravity modeling along the profile aa' in the T1 region (Figures 17c and 19a). The oceanic crust in the T1 region is about 8–12 km thick, which is a little thicker than the normal oceanic crust (6–8 km). The extremely thin crust near the Manila Trench may be an artifact caused by incorrect subduction-related crust model (Figure 19a). The NE–SW trend of the Bouguer anomaly is roughly parallel to the Manila Trench (Figure 17c) but is oblique to the E–W trend of the magnetic lineation in the northernmost SCS (Figure 1). Some distributed seamounts also display NE–SW trends (Figure 1). Accordingly, it implies that the crustal thickness of the northern SCS may be partly controlled by the southeastward rifting of the continental margin or more possibly due to southeastward upper mantle flow in this region.

To understand the crustal variation across the LRTPB, we have performed gravity modeling along the profiles bb' and cc' in Figure 17c. The water density $\rho_w = 1.03$ g/cm^3, sediment density $\rho_s = 2.2$ g/cm^3, the crust density $\rho_c = 2.85$ g/cm^3

and mantle density $\rho_m = 3.3$ g/cm^3 are used (cf. Nissen et al., 1995; Chi et al., 2003). The gravity modeling has been done in the sense of least square error between the observed and the synthetic Bouguer anomalies (Figures 19b and c). The gravity modelings along the profiles bb' and cc' show that beneath the LRTPB the crust is relatively thin (Figures 19b and c). It agrees that the location of the LRTPB is a trace of a transform fault. The region T2 (region tc in Figures 19b and 19c) has larger Bouguer anomaly than the T1 region (Figure 17c). It can be interpreted either a higher density material in the crust or a rather thin crust when the normal density is used in the modeling. The reason for the high Bouguer in the T2 region remains unclear. The region T3 (tps in Figure 19c) has similar crustal thickness as in the T1 region (SCS oceanic crust). It is interesting to note that beneath the Formosa Canyon the crust is dramatically thick (Figure 19c). This phenomenon could be attributed to the SCS post-spreading volcanic intrusion as indicated by Sibuet et al. (2002) in this area or by Ludmann and Wong (1999) in the Dongsha Rise area.

Conclusions

We have presented 20 multi-channel seismic profiles and performed gravity modeling in the northernmost SCS. Based on the seismic interpretation and gravity analysis, we can draw the following conclusions:

1. The crust in the northernmost SCS is generally thinner from NW to SE; the oceanic crust is mainly of 8–12 km thick. Some local thick oceanic crust may be caused by post-spreading volcanism. The oceanic crust of the northern SCS is limited in the north by the NW–SE trending LRTPB.
2. The crust beneath the LRTPB is relatively thin, in agreement with the character of a transform fault. However, the shearing features in the volcanic basement along the LRTPB can only be observed at the both ends of the LRTPB, where the gravity anomalies are relatively low.
3. The LRTPB is not an active fault or sheared zone. The seismic sequences directly above the LRTPB have not been faulted but have only displayed differential subsidence across the LRTPB. Some normal faults in the upper layers have

occurred along the southeast portion of the LRTPB, near the Manila Trench.

4. Normal faults cutting through the whole sedimentary layers can be observed at the southeast end of the study profiles, close to the Manila Trench. The faulting is probably due to bending of the subducting SCS lithosphere.

5. The Formosa Canyon has developed along the northwestern portion of the LRTPB and changed its course from NW–SE trend to E–W trend near seamount H. Seafloor erosion has occurred extensively along the entire channel of the Formosa Canyon.

Acknowledgement

References

Briais, A., Patriat P. and Taponnier, P., 1993, Updated interpretation of magnetic anomalies and seafloor spreading stages in South China Sea: Implications for the Tertiary tectonics of Southeast Asia, *J. Geophys. Res.* **98**, 6299–6328.

Chen, S., 1987, Magnetic profiles, in Atlas of Geology and Geophysics of the South China Sea, scale 1:2000,000, *Second Mar. Geol. Invest. Brigade of the Minist. of Geol. and Miner. Resour., Guangdong Province*, Guangdong.

Chi, W.-C., Reed, D.L., Moore, G., Nguyen, T., Liu C.-S. and Lundberg, N., 2003, Tectonic wedging along the rear of the offshore Taiwan accretionary prism, *Tectonophysics* **374**, 199–217.

Hsu, S.-K. and Sibuet, J.-C., 1995, Is Taiwan the result of arc-continental or arc-arc collision?, *Earth Planet. Sci. Lett.* **136**, 315–324.

Hsu, S.-K., Liu, C.-S., Shyu, C.-T., Liu, S.-Y., Sibuet, J.-C., Lallemand, S., Wang, C. and Reed, D., 1998, New gravity and magnetic anomaly maps in the Taiwan-Luzon region and their preliminary interpretation, *TAO* **9**, 509–532.

Hsu, S.-K., Yeh, Y.-C., Doo W.-P. and Tsai, C.-H., 2005, New bathymetry and magnetic lineations identifications in the northernmost South China Sea and their tectonic implications, (MGR, this issue).

Lallemand, S. et al., 1997, Swath bathymetry reveals active arc-continent collision near Taiwan, *EOS, Trans, AGU* **78**, 178–175.

Lin, A.-T. and Watts, A.-B., 2002, Origin of the West Taiwan basin by orogenic loading and flexure of a rifted continental margin, *J. Geophys. Res.* **107**, B9, 2185.

Liu, C.-S., Liu, S.-Y., Lallemand, S., Lundberg, N. and Reed, D.L., 1998, Digital elevation model offshore Taiwan and its tectonic implications, *TAO* **9**, 705–738.

Ludmann, T. and Wong, H.-K., 1999, Neotectonic regime on the passive continental margin of the northern South China Sea. *Tectonophysics* **311**, 113–138.

Nissen, S.-S., Hayes, D.-E., Yao, B., Zeng, W., Chen, Y. and Nu, X., 1995, Gravity, heat flow, and seismic constraints on the process of crustal extension: Northern margin of the South China Sea, *J. Geophys. Res.* **100**, 22447–22483.

Sibuet, J.-C. and Hsu, S.-K., 1997, Geodynamics of the Taiwan arc-arc collision, *Tectonophysics* 274, 221–251.

Sibuet, J.-C., Hsu, S.-K., Le Pichon, X., Le Formal, J.-P., Reed, D., Moore, G. and Liu, C.-S., 2002, East Asia plate tectonics since 15 Ma: Constraints from the Taiwan region, *Tectonophysics* **344**, 103–134.

Sibuet, J.-C. and Hsu, S.-K., 2004, How was Taiwan created?, *Tectonophysics* **379**, 159–181.

Taylor, B. and Hayes, D. E., 1980, The tectonic evolution of the South China Basin, in Hayes, D. E. (ed.), *The Tectonic and Geologic Evolution of Southeast Asian Seas and Islands*, 1, Washington, DC: American Geophysical Union, pp. 23–56.

Taylor, B. and Hayes, D. E., 1983, Origin and history of the South China Sea Basin, in Hayes, D. E. (ed.), *The Tectonic and Geologic Evolution of Southeast Asian Seas and Islands*, 2, Washington, DC: *American Geophysical Union*, pp. 23–56.

Tsai, C.-H., Hsu, S.-K., Yeh Y.-C. and Lee, C.-S., 2005, The crustal structures of northern continental margin in the South China Sea, 2005, (MGR, this issue).

Wessel, P., and Smith, W. H. F., 1998, New improved version of Generic Mapping Tools released, *EOS Trans. AGU* **79**, 579.